Research Square

Preprints are preliminary reports that have not undergone peer review.
They should not be considered conclusive, used to inform clinical practice,
or referenced by the media as validated information.

Formability and Microstructure of Dissimilar Aluminium Tailor-Welded Blanks (TWBs) Joined using Friction Stir and Gas Tungsten Arc Welding

Hamidreza Rezaei Ashtiani

hr_rezaei@arakut.ac.ir

Arak University of Technology https://orcid.org/0000-0001-8500-1421

Davood Bagheri

Arak University of Technology

Research Article

Keywords: Friction Stir Welding (FSW), Gas Tungsten Arc Welding (GTAW), Forming Limit Diagram (FLD), Aluminium alloy sheet, Tailor Welded Blank (TWB)

Posted Date: November 2nd, 2026

DOI: https://doi.org/10.21203/rs.3.rs-11170399/v1

License: This work is licensed under a Creative Commons Attribution 4.0 International License.
Read Full License

Formability and Microstructure of Dissimilar Aluminium Tailor-Welded Blanks (TWBs) Joined using Friction Stir and Gas Tungsten Arc Welding

Hamidreza Rezaei Ashtiani*, Davood Bagheri
School of Mechanical Engineering, Arak University of Technology, Arak, 38135-1177, Iran.

Abstract

In this study, to evaluate the performance of different welding techniques in joining dissimilar aluminum alloys, known as the Tailor Welded Blank (TWB) concept, and to investigate their resulting mechanical properties and microscopic structures, three aluminium alloys—AA3105, AA5052, and AA1200—were investigated. These alloys were joined as multi-material dissimilar blanks using Gas Tungsten Arc Welding (GTAW) and Friction Stir Welding (FSW). By conducting Nakazima formability tests on the welded specimens, forming limit diagrams (FLD) were extracted. The FLD indicated that, across the strain paths examined, the FSW joints generally showed higher forming-limit strains and a broader safe-forming region than the corresponding GTAW joints. FSW 1–5 displayed the greatest formability, while AA5052 exhibited the lowest overall forming ability. The improved formability of the FSW joints suggests the feasibility of solid-state welding for producing dissimilar aluminium sheets that will undergo subsequent forming operations. The FSW 1–5 joint exhibited approximately 152% higher displacement capacity than the corresponding TIG joint during Nakazima testing.

Keywords: Friction Stir Welding (FSW), Gas Tungsten Arc Welding (GTAW), Forming Limit Diagram (FLD), Aluminium alloy sheet, Tailor Welded Blank (TWB).

* Corresponding author at: *School of Mechanical Engineering, Arak University of Technology, Arak, 38135-1177, Iran. Tel.: +98 861 3670024; Fax: +98 861 3670020.*
E-mail address: hr_rezaei@arakut.ac.ir (*H.R. Rezaei Ashtiani*)
ORCID: 0000-0001-8500-1421

1. Introduction

The increasing demand for lightweight structures with enhanced mechanical performance has accelerated the development of advanced joining technologies for aluminium alloys. In industries such as automotive, aerospace, railway transportation, and shipbuilding, the fabrication of reliable welded joints is essential for reducing structural weight while maintaining adequate strength, durability, and formability. Consequently, significant research efforts have been devoted to developing joining techniques that produce high-quality welds with minimal defects and superior mechanical performance. Among the available joining processes, fusion welding and solid-state welding represent the two principal categories for joining sheet metals. Gas Tungsten Arc Welding (GTAW), commonly referred to as Tungsten Inert Gas (TIG) welding, is one of the most widely used fusion welding techniques because of its excellent weld quality, high dimensional accuracy, and superior surface finish. In the GTAW process, an electric arc is established between a non-consumable tungsten electrode and the workpiece, generating sufficient heat to melt the base material. The weld pool is protected from atmospheric contamination by an inert shielding gas, typically argon, helium, or their mixtures. Although GTAW can produce high-quality welds, the relatively high heat input often leads to excessive distortion, residual stresses, grain coarsening, and degradation of mechanical properties, particularly in thin aluminium sheets with thicknesses below approximately 2 mm [1].

Friction Stir Welding (FSW), introduced by The Welding Institute (TWI) in 1991, has emerged as one of the most successful solid-state joining technologies for aluminium alloys. Unlike fusion welding processes, FSW joins materials below their melting temperature using a rotating non-consumable tool consisting of a shoulder and a profiled pin. During welding, frictional heating and severe plastic deformation soften the surrounding material. Simultaneously, the rotating tool transports the plasticized material from the advancing side to the retreating side, producing a consolidated joint through dynamic recrystallization. Because melting is avoided, FSW significantly reduces welding defects such as porosity, hot cracking, solidification shrinkage, and excessive distortion. Furthermore, the absence of filler materials and shielding gases, together with its relatively low energy consumption, makes FSW an environmentally friendly and economically attractive joining process for high-volume manufacturing applications [2].

The formability of welded sheet metals is a critical consideration in the manufacturing of lightweight components. Formability describes the ability of a sheet material to undergo plastic deformation without localized necking or fracture during forming operations. Among the available characterization methods, the Forming Limit Diagram (FLD) is widely accepted as the standard criterion for evaluating sheet metal formability. The FLD defines the combinations of major and minor principal strains corresponding to the onset of localized necking, thereby distinguishing the safe forming region from the failure region. In the present study, the FLD was determined using the standardized Nakazima out-of-plane stretching test, in which a circular grid pattern is applied to the specimen surface before deformation. Following deformation, the deformation of the circular grid elements into ellipses is measured to calculate the major and minor principal strains and subsequently construct the forming limit curve (FLC) [3].

Extensive research has been conducted on the mechanical behavior, microstructural evolution, and formability of welded aluminum alloys produced by different joining techniques [4–26]. Comparative investigations involving GTAW, Gas Metal Arc Welding (GMAW), Laser Beam Welding (LBW), and FSW have consistently demonstrated that the welding process significantly influences the resulting microstructure and mechanical performance. For example, studies on AA6061 joints produced by GTAW, GMAW, and FSW reported that GMAW achieved higher joint efficiency than the other two welding methods under the investigated conditions [6]. In contrast, comparative studies on AA2014-T6 indicated that FSW produced superior tensile properties and joint quality owing to the elimination of solidification-related defects commonly associated with fusion welding [14]. Similarly, Edip et al. [15] investigated dissimilar welding of AA5182 and AA7075 alloys using GTAW and GMAW, demonstrating that both processes produced comparable mechanical properties when appropriate welding parameters and groove geometries were employed. Moreover, investigations on AA1050 aluminum sheets revealed that FSW joints exhibited superior mechanical performance and more uniform strain distribution than those produced by GTAW [16].

Considerable attention has also been devoted to evaluating the formability of welded aluminum tailor-welded blanks through experimental and numerical approaches [27–38]. Previous studies have shown that the forming behavior of welded sheets is strongly affected by the welding technique, welding parameters, material combination, and loading condition. For instance,

comparative investigations on AA6061 tailor-welded blanks joined by FSW, Friction Stir Vibration Welding (FSVW), and CO_2 laser welding demonstrated that FSVW provided the highest forming limits and limiting dome heights among the investigated joining methods [27]. Studies on dissimilar AA5182-AA6061 FSW tailor-welded blanks further revealed that both the material arrangement and welding parameters significantly influence the forming limit, with optimum performance obtained at a rotational speed of 700 rpm and a traverse speed of 150 mm min^{-1} [28]. Other investigations have shown that elevated forming temperatures substantially improve the FLD of aluminum alloys and stainless steels, whereas factors such as sheet orientation, punch geometry, strain path, and geometric discontinuities also play important roles in determining formability [29–34]. More recently, Deilami and Safari [32] demonstrated that increasing the rotational speed during FSW reduced the formability of ultra-thin steel tailor-welded blanks, whereas increasing the welding speed improved their forming performance.

Although numerous studies have investigated the mechanical properties, microstructural evolution, and formability of welded aluminum alloys, most have focused on similar-material joints or a single welding technique. Comparative investigations evaluating the formability of dissimilar aluminum tailor-welded blanks produced by both fusion welding and solid-state welding remain limited. In particular, comprehensive FLD-based studies involving AA5052-AA3105 and AA5052-AA1200 dissimilar joints are rarely reported in the literature. Furthermore, the combined effects of welding process, weld quality, and microstructural characteristics on the forming behavior of these dissimilar aluminum combinations have not yet been fully clarified.

Therefore, the present study aims to comparatively investigate the formability of dissimilar aluminum tailor-welded blanks fabricated from AA5052-AA3105 and AA5052-AA1200 alloys using Friction Stir Welding (FSW) and Gas Tungsten Arc Welding (GTAW). Formability was evaluated using the Nakazima test by constructing forming limit diagrams, while the corresponding failure characteristics, mechanical behavior, and microstructural evolution of the welded joints were systematically analyzed. The findings provide a comprehensive assessment of the influence of welding technique on the forming performance of dissimilar aluminum tailor-welded blanks and offer useful guidance for the manufacturing of lightweight sheet-metal components.

2. Materials and Experimental Procedure

Sheets of AA1200, AA5052, and AA3105 aluminum alloys, each with a thickness of 2 mm, were used to fabricate dissimilar tailor-welded blanks. Two material combinations, AA3105–AA5052 and AA1200–AA5052, were produced using both FSW and GTAW. Nakazima formability tests were conducted in accordance with ISO 12004-2 to construct the forming limit curves.

The chemical compositions of the alloys are presented in Tables 1–3, and their initial microstructures are shown in Figure 1. The average grain sizes were determined to be 30–40 µm for AA1200, 150–200 µm for AA3105, and 40–50 µm for AA5052.

Table 1: Chemical composition of AA 5052 alloy (wt.%).

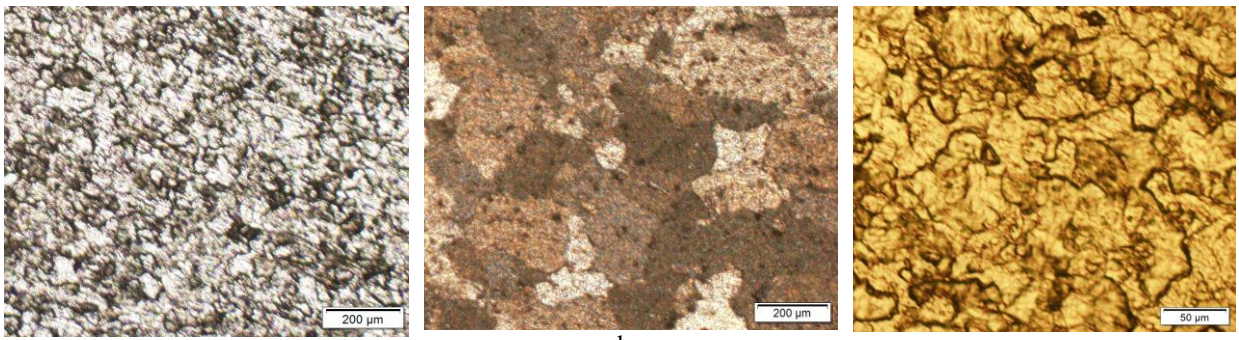
Mg	Cr	Si	Fe	Cu	Mn	Zn	Others	Al
2.2-2.8	0.15-0.35	< 0.25	< 0.4	< 0.1	< 0.1	< 0.1	< 0.15	Rem

Table 2: Chemical composition of AA 3105 alloy (wt.%).

Mg	Cr	Si	Fe	Cu	Mn	Zn	Ti	Others	Al
0.2-0.8	< 0.2	< 0.6	< 0.7	< 0.3	0.3-0.8	< 0.4	< 0.1	< 0.15	Rem

Table 3: Chemical composition of AA 1200 alloy (wt.%).

Si+Fe	Cu	Mn	Zn	Ti	Others	Al
< 1	< 0.05	< 0.05	< 0.1	< 0.05	< 0.15	Rem



a b c

Figure 1. Microstructures of a) AA 1200, b) AA 3105, and c) AA 5052.

GTAW was performed manually, and process parameters, including welding current (100–120 A) and filler metal diameter, were systematically evaluated. For FSW, the selection and optimization of rotational speed, traverse speed, and tool tilt angle were guided by preliminary trials and recommendations from the literature. In the FSW trials, rotational speeds of 1200, 1600, and 2000 rpm, traverse speeds of 8, 12, and 20 mm min^{-1}, and tool tilt angles ranging from 1° to 2° were examined. FSW butt-joint specimens were clamped in a rigid fixture and welded using a tool machined from H13 hot-work tool steel. FSW was carried out on an FP4M milling machine, whereas GTAW was performed using a TRIPLE 500 welding unit (Figure 2).

The geometry and dimensions of the FSW tool are shown in Figure 3. Abbreviated designations were adopted to simplify specimen identification, as summarized in Table 4.



a b

Figure 2. Experimental equipment a) GTAW setup, and b) Milling machine utilized for FSW.

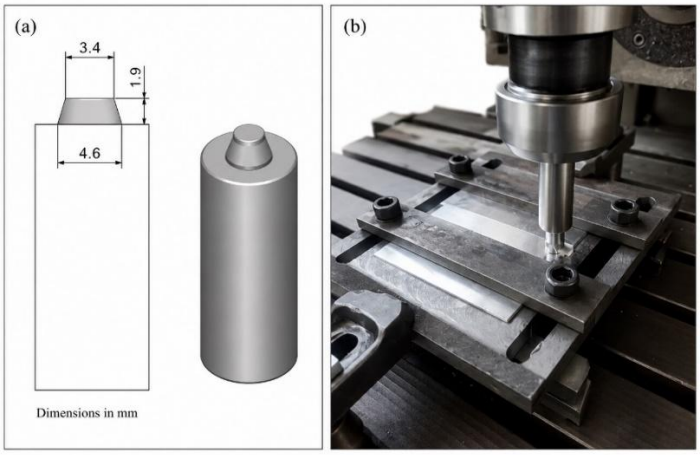


Figure 3. (a) Schematic diagram and dimensions and (b) experimental condition of the FSW tool.

Table 4: Nomenclature and designation of experimental specimens.

No.	Designation	Description
1	AA1200	As-received AA1200 base metal sheet
2	AA5052	As-received AA5052 base metal sheet
3	AA3105	As-received AA3105 base metal sheet
4	FSW 1-5	FSW dissimilar joint: AA1200 – AA5052
5	FSW 3-5	FSW dissimilar joint: AA3105 – AA5052
6	TIG 1-5	GTAW dissimilar joint: AA1200 – AA5052
7	TIG 3-5	GTAW dissimilar joint: AA3105 – AA5052

Out-of-plane Nakazima tests were performed in accordance with ISO 12004-2 using a sub-size die configuration consisting of a blank holder and a hemispherical punch with a diameter of 44 mm. The die was machined from MO40 alloy steel and heat-treated to a hardness of approximately 40 HRC. Figure 4 shows the die geometry and dimensions. The two-piece die assembly was aligned using precision guide pins and secured with four socket-head cap screws. A guide sleeve in the upper die housing ensured accurate punch alignment. Specimens with different waist widths were prepared using wire electrical discharge machining (wire-EDM) to generate a range of strain paths. The specimen geometries and the gridded specimens used for Nakazima testing are shown in Figure 5, and representative prepared specimens are shown in Figure 6. Before forming, a circular grid pattern was applied to the specimen surfaces to evaluate the surface strain distribution after deformation. The pattern was transferred using a gelatin stamp with raised grid features coated with specialized ink.

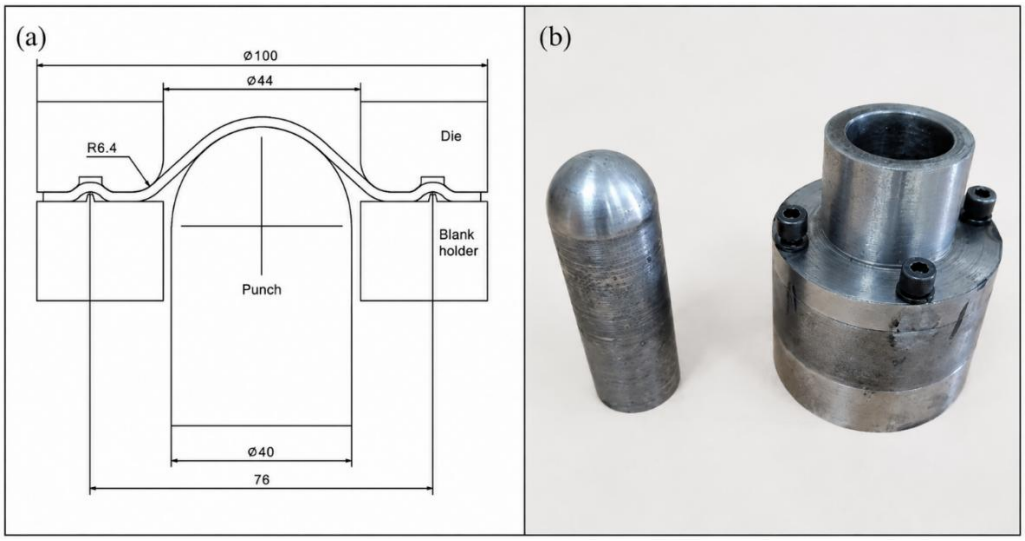


Figure 4. Tooling setup for the Nakazima test: a) Assembly schematic, and b) Die components

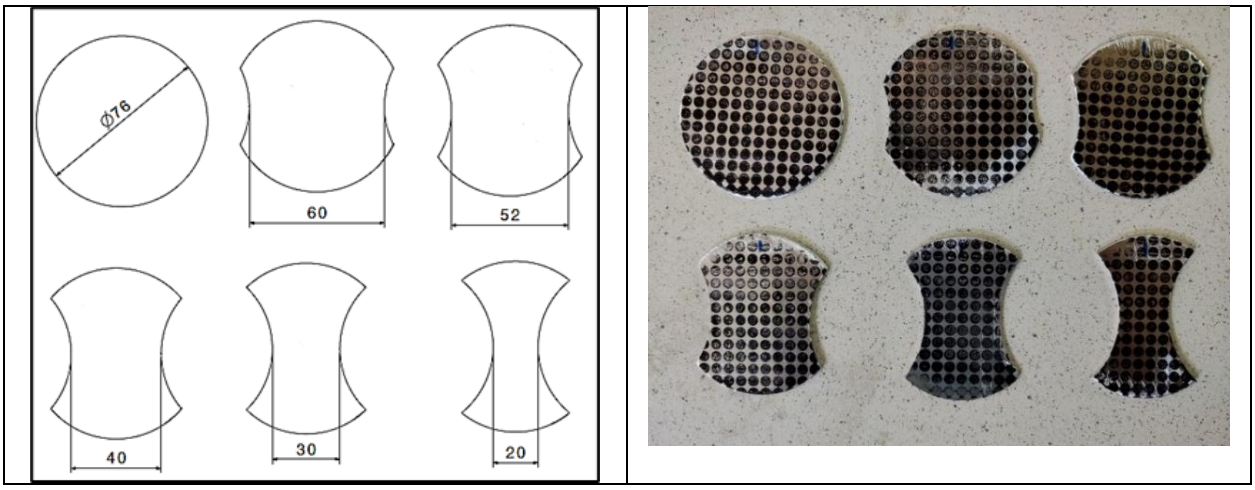


Figure 5. Geometries and dimensions of gridded specimens for Nakazima formability testing.

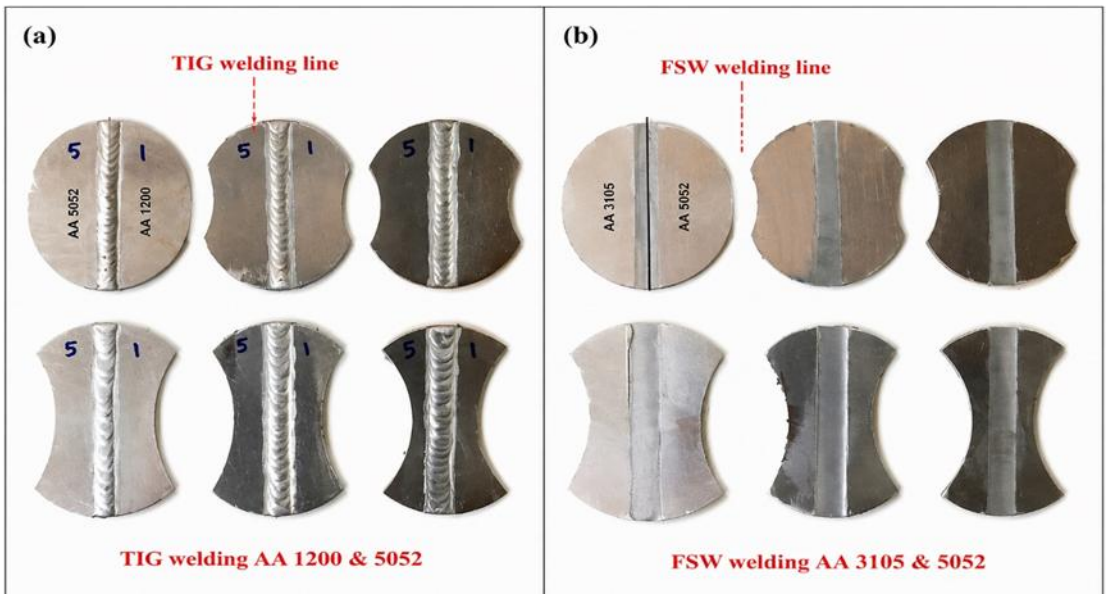


Figure 6. Wire-EDM-prepared TIG and FSW welded specimens for Nakazima test.

After Nakazima testing, the major and minor axes of the deformed circular grid elements were measured using a Mylar scale. Major true strain (ε_1) and minor true strain (ε_2) were calculated using Equation (1).

The engineering limit strains are expressed as:

$$e_1 = \frac{D - d_\circ}{d_\circ} \qquad e_2 = \frac{d - d_\circ}{d_\circ} \tag{1}$$

where e_1 is the major engineering strain, e_2 is the minor engineering strain, D is the major axis of the deformed ellipse, d is the minor axis, and d_0 is the initial circle diameter.

The true limit strains are calculated using:

$$\varepsilon_1 = ln\frac{D}{d_\circ} \qquad \varepsilon_2 = ln\frac{d}{d_\circ} \tag{2}$$

where ε_1 is the major true strain, ε_2 is the minor true strain, D is the major axis, d is the minor axis, and d_0 is the initial circle diameter.

To analyze formability behavior, tracking the deformation path is essential. The strain path reflects the ratio of minor strain (ε_2) to major strain (ε_1) throughout deformation. This relationship is quantified by the strain path parameter α:

$$\alpha = \frac{\varepsilon_2}{\varepsilon_1} \quad (3)$$

where ε_2 and ε_1 represent the minor and major true strains, respectively. Based on the magnitude of α, the strain state is classified as: $\alpha<0$: Uniaxial tension domain, $\alpha=0$: Plane strain domain, and $\alpha>0$: Equi-biaxial tension domain.

3. Results and Discussion

The optimized FSW parameters were identified as a tool rotational speed of 1600 rpm, a traverse speed of 12 mm min^{-1}, and a tool tilt angle of 1.5°. For GTAW, the optimized condition consisted of a welding current of 120 A with a 2.4-mm-diameter ER5356 aluminum filler rod. Representative welded specimens produced by FSW and GTAW are shown in Figure 7. After Nakazima testing, strain analysis was performed using a Mylar scale, as shown in Figure 8, and forming limit curves were constructed.

Figure 9 presents the forming limit diagram for the AA3105 base material. The region below the FLC represents the safe forming region, whereas strain states above the curve indicate localized necking and fracture.

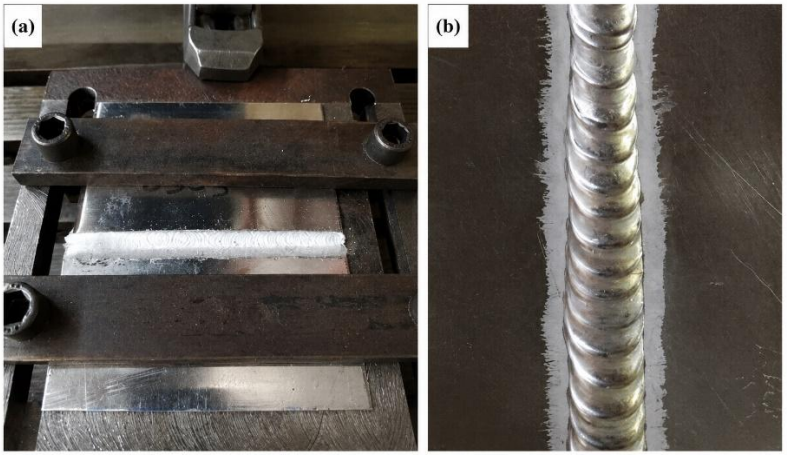


Figure 7: Welded joint appearances: a) FSW specimen, and b) GTAW specimen.



Figure 8: Deformed specimen following Nakazima formability testing.

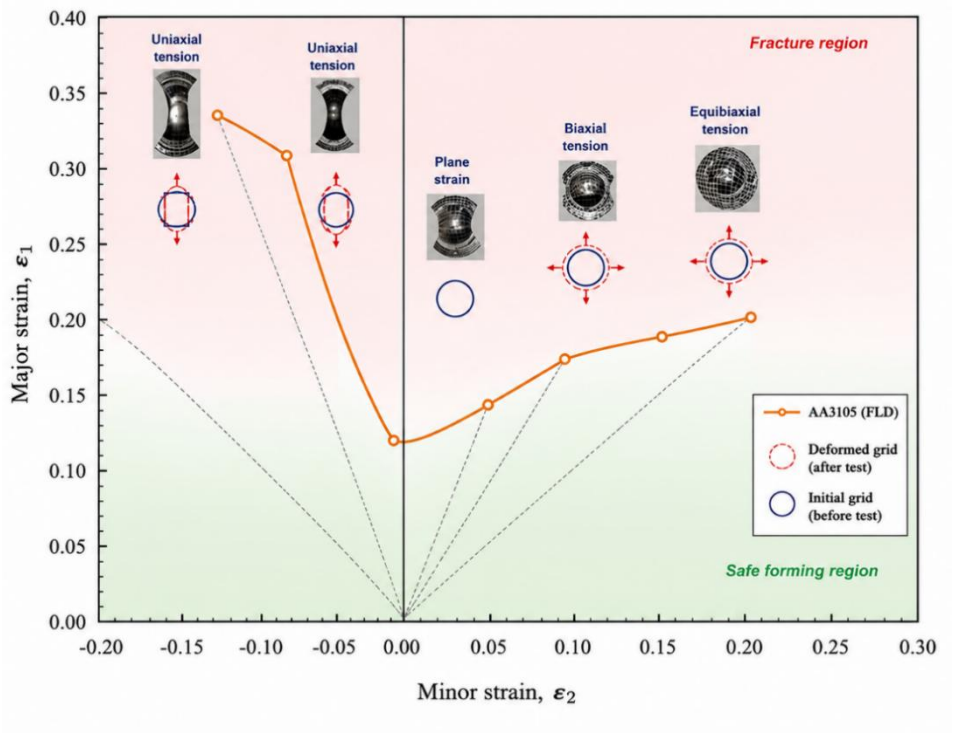
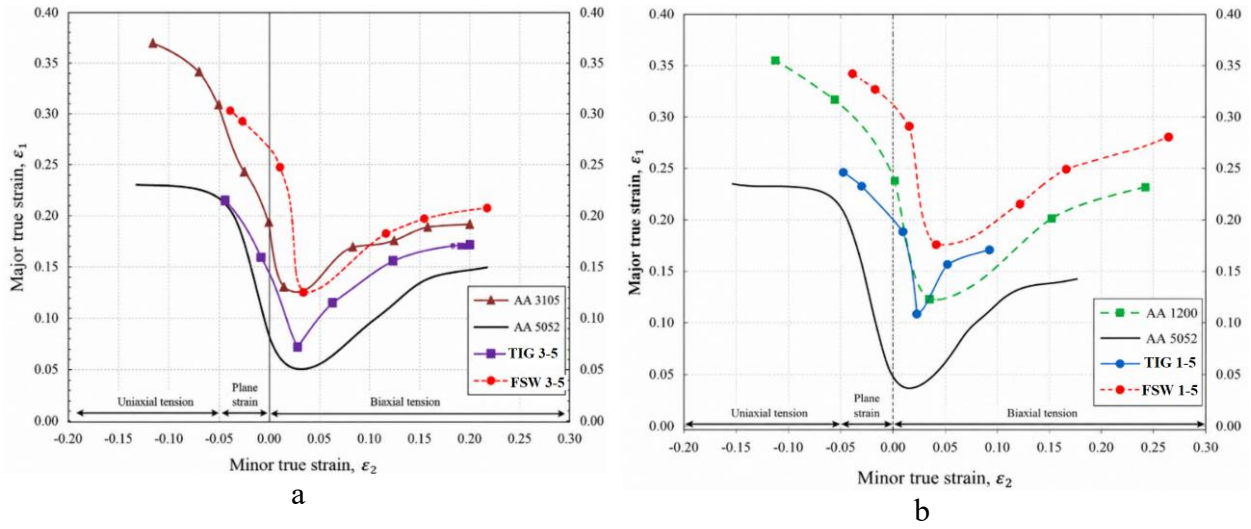


Figure 9: Forming Limit Diagram for AA 3105 base alloy.

Figure 10 compares the forming limit diagrams of GTAW- and FSW-welded specimens against the base metals. AA 5052 exhibits the lowest overall formability, whereas the FSW 1-5 joint

displays the highest formability limit. Overall, FSW joints demonstrate superior forming capacity compared to GTAW joints. Figure 11 depicts the variation of limit strains across different strain paths ($\alpha=\varepsilon_2/\varepsilon_1$). The horizontal axis denotes the strain ratio α, while the vertical axis represents the major limit strain (ε_1). The plots cover uniaxial tension, plane strain, biaxial tension, and mixed strain paths.

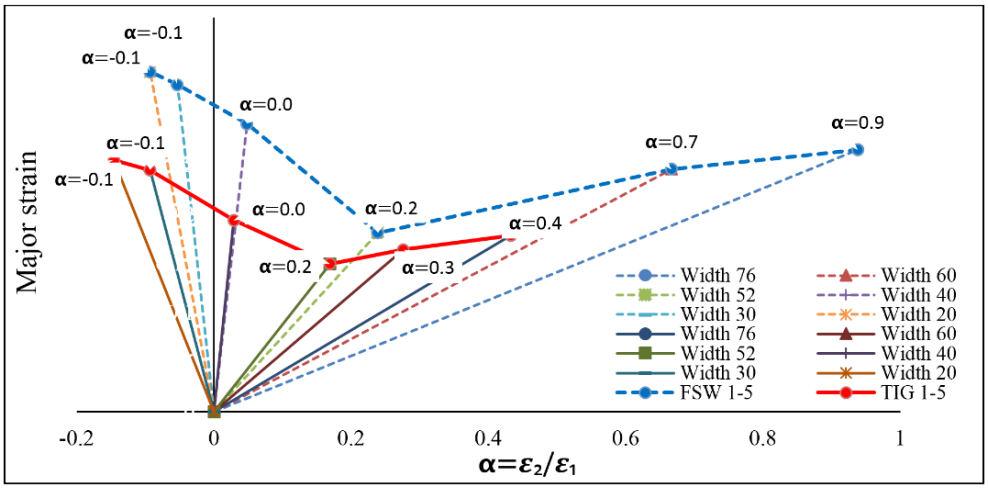


a b

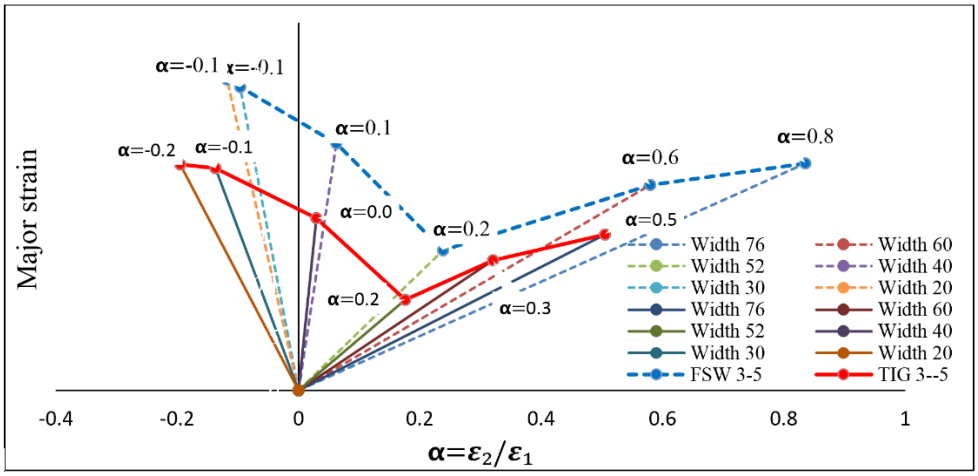
Figure 10: Comparison of forming limit curves for welded specimens and base metals: a) TIG 3-5 (T3-5) vs. FSW 3-5 (F3-5), and b) TIG 1-5 (T1-5) vs. FSW 1-5 (F1-5).

Figure 12 depicts the variation of limit strains across different strain paths ($\alpha=\varepsilon_2/\varepsilon_1$). The horizontal axis denotes the strain ratio α, while the vertical axis represents the major limit strain (ε_1). The plots cover uniaxial tension, plane strain, biaxial tension, and mixed strain paths. The FSW 1–5 joint extended the investigated strain-path range from α = 0.4 for TIG 1–5 to α = 0.9, corresponding to an absolute increase of 0.5 in α and a 125% increase relative to the TIG joint. The FSW 1–5 joint demonstrated a substantially broader biaxial strain-path coverage, reaching α = 0.9, whereas the TIG 1–5 joint reached only α = 0.4. The maximum investigated strain-path parameter increased from α = 0.5 for TIG 3–5 to α = 0.8 for FSW 3–5, corresponding to an absolute increase of 0.3 and a 60% increase relative to the TIG joint. The investigated α-range was 0.9 for FSW 3–5 and 0.7 for TIG 3–5, indicating a 28.6% broader strain-path range for the FSW joint. FSW 3–5 provided broader coverage toward the positive biaxial-tension regime, whereas TIG 3–5 extended further toward negative minor-strain conditions.

ای



a



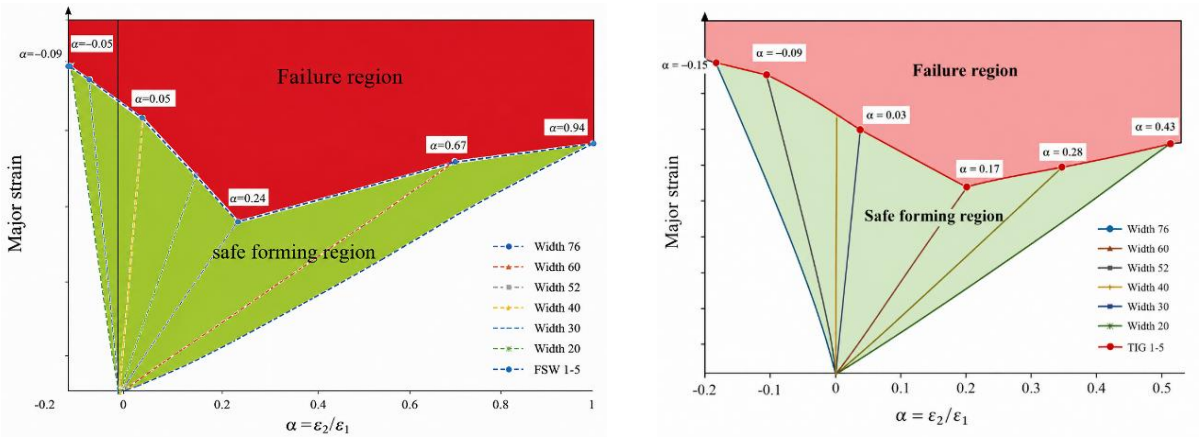
b

Figure 11: Forming limit variation vs. principal strain ratio ($\alpha=\varepsilon_2/\varepsilon_1$) for welded specimens: a) FSW 1-5 vs. TIG 1-5, and b) FSW 3-5 vs. TIG 3-5.

The comparative curves confirm that FSW joints consistently outperform GTAW joints across all strain paths. FSW limit curves reside at significantly higher strain levels, indicating that the fine, equiaxed dynamic recrystallized grain structure produced during solid-state stirring enhances sheet formability. The comparative curves confirm that FSW joints consistently outperform GTAW joints across all strain paths. FSW limit curves reside at significantly higher strain levels, indicating that the fine, equiaxed dynamic recrystallized grain structure produced during solid-state stirring

enhances sheet formability. The safe and fracture domains illustrated in Figure 12 compare the forming windows for FSW and GTAW aluminium joints. FSW specimens display an expanded safe forming window with higher limit strain boundaries, whereas GTAW specimens exhibit premature necking and a constricted safe window. The FSW 1–5 joint extended the investigated strain-path range to α = 0.94, corresponding to 94% of the equibiaxial strain-path condition (α = 1). The safe-forming region of the FSW 1–5 joint extended over a broad strain-path range from α = −0.09 to α = 0.94. Notably, the upper boundary approached the equibiaxial strain condition (α = 1), reaching 94% of the corresponding strain-path ratio.

The enhanced formability of the FSW joints can be attributed to greater microstructural homogeneity, more uniform strain distribution, and reduced stress concentrations compared with fusion-welded joints. Consequently, FSW preserves the formability of tailor-welded blanks more effectively than GTAW. Figure 13 compares the force–displacement response curves of FSW and GTAW specimens with those of the base metals during Nakazima testing. The FSW specimens, particularly FSW 1-5, sustained the largest displacement before failure, indicating greater overall ductility.



(a) (b)

Figure 12: Comparison of safe and failure regions during forming for specimens welded by: a) FSW, and b) GTAW (TIG).

In GTAW joints, complete melting and subsequent solidification promote coarse dendritic structures in the fusion zone and heat-affected zone (HAZ), accompanied by solidification defects such as porosity and micro-cracking that exacerbate stress concentrations and impair plastic

deformability. Conversely, solid-state FSW avoids liquid-to-solid phase transformations, relying on dynamic recrystallization to refine the microstructure, enhance metallurgical bonding, and eliminate solidification defects. This refined microstructure delays crack initiation and propagation, enabling higher strains prior to ductile failure.

Figure 13 presents the force-displacement curves of welded specimens and base metals during dome testing and a cross-sectional metallographic overview of the FSW 3-5 joint, respectively. The stir zone (SZ) is distinctly refined compared to the base metal (BM) due to severe plastic deformation and thermal exposure, with clear interface boundaries reflecting microstructural gradients across the thermo-mechanically affected zone (TMAZ) and HAZ. The curved interface morphology indicates complex material flow during stirring. High-magnification micrographs (Figure 14) show significant grain refinement in the stir zone compared to the base metal.

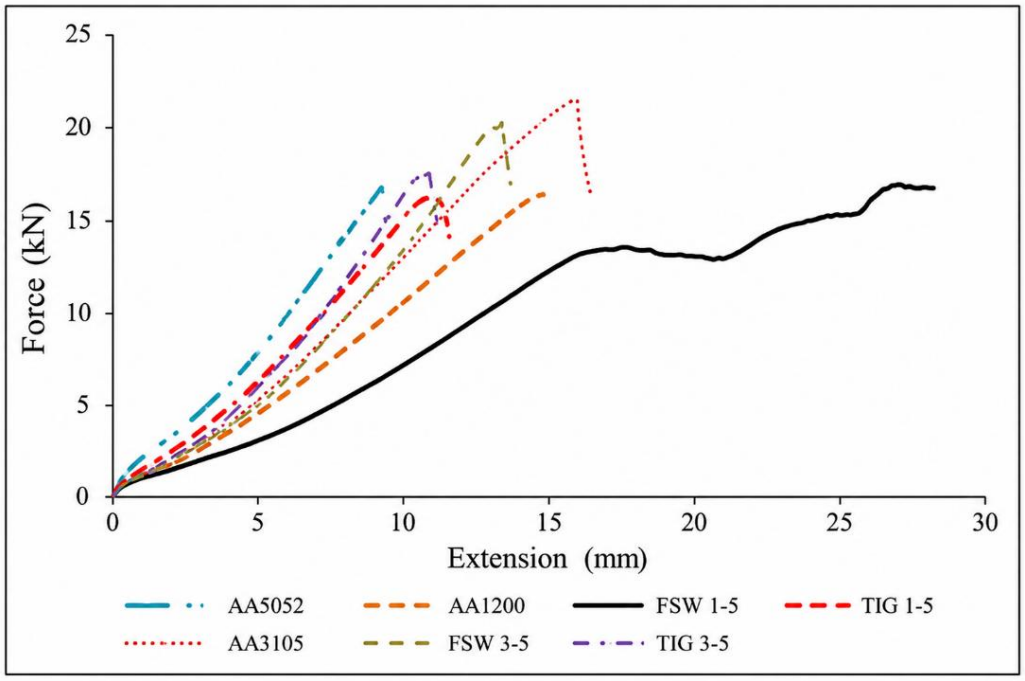


Figure 13: Force-displacement curves of welded specimens and base metals during dome testing.

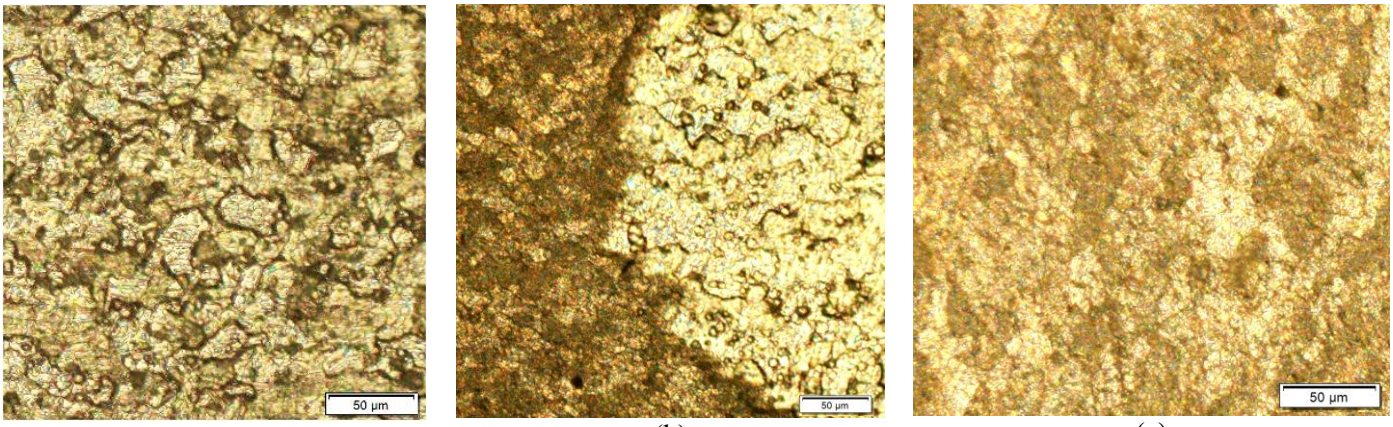
Figure 14 shows a cross-sectional metallographic overview of the FSW 3-5 joint. The central stir zone (SZ) is clearly demarcated from the adjacent base metals: AA 3105 on the left and AA 5052 on the right. The SZ features a distinct refined structure compared to the base metal (BM) due to

severe plastic deformation and thermal exposure. Distinct interface boundaries reflect microstructural gradients across the thermo-mechanically affected zone (TMAZ) and HAZ. The characteristic curved interface morphology reflects complex material flow patterns during stirring.

Figure 15 presents high-magnification micrographs (200X) across different joint regions. Micrograph (b) highlights substantial grain refinement in the stir zone relative to the base metal microstructures.



Figure 14: Cross-sectional optical micrograph of the FSW 3-5 joint.



(a) (b) (c)

Figure 15: Optical micrographs of a) AA5052 base metal, b) Stir zone (SZ), and c) AA3105 base metal.

Figure 16 illustrates post-test failure locations in formed Nakazima specimens. FSW specimens fractured outside the stir zone, propagating along the transition interface near the weaker base metals (AA3105 / AA1200). Conversely, GTAW specimens failed within or near the weld seam due to fusion defects and coarse grain structures.

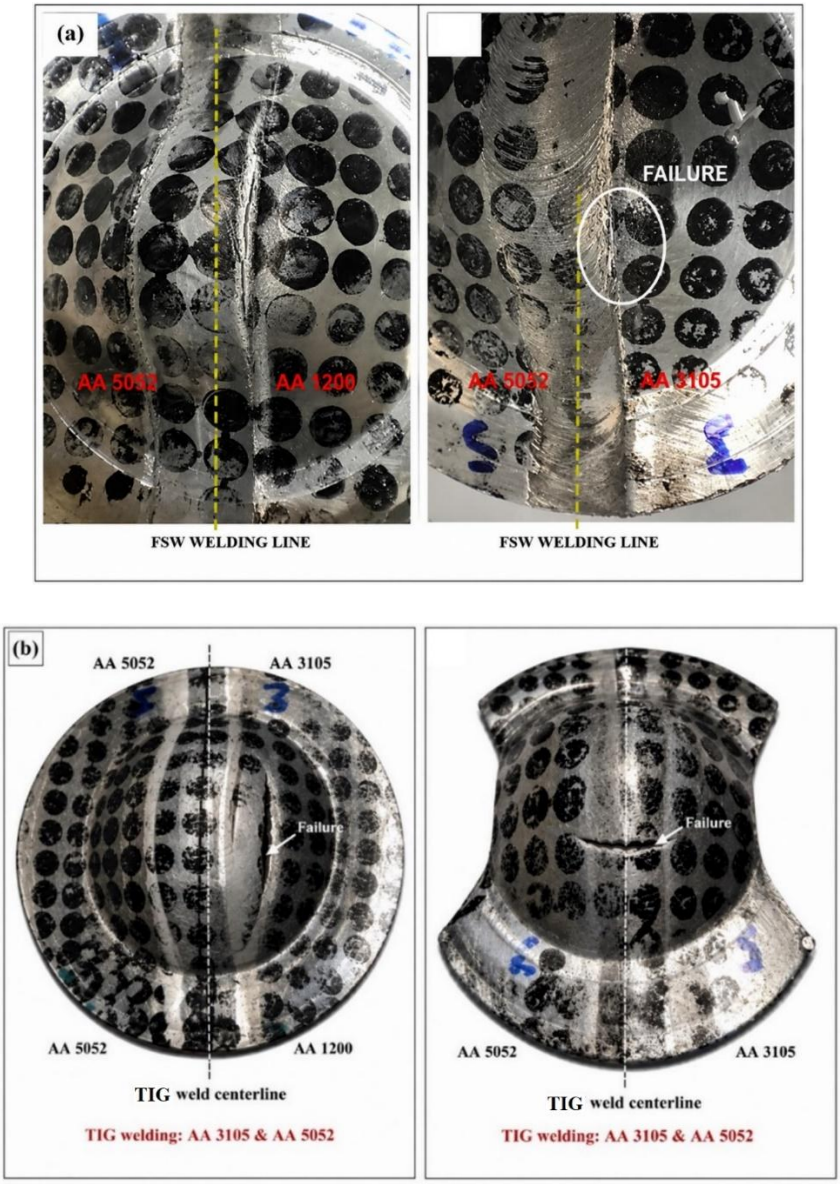


Figure 16: Post-forming failure locations in specimens welded by a) FSW and b) GTAW.

4. Conclusions

This study experimentally investigated the influence of friction stir welding (FSW) and gas tungsten arc welding (GTAW) on the formability, deformation behavior, microstructure, and failure characteristics of dissimilar aluminium sheets. The AA5052–AA3105 and AA5052–AA1200 joints were evaluated using Nakazima forming tests, forming limit diagrams (FLD),

force–displacement measurements, and metallographic characterization. The main conclusions are as follows:

- FSW produced higher forming-limit strains and a wider safe-forming region than the corresponding TIG joints under the investigated conditions as the FSW 1–5 joint exhibited approximately 152% higher displacement capacity than the corresponding TIG joint during Nakazima testing.
- The enhanced formability of FSW joints was associated with the refined and relatively homogeneous stir-zone microstructure produced by severe plastic deformation and dynamic recrystallization.
- Failure predominantly occurred outside the FSW stir zone, whereas TIG specimens failed within or near the fusion-weld region, indicating different strain-localization and damage-development mechanisms, further confirming the superior deformation capability of the FSW joints.
- Among the conditions investigated, FSW 1–5 displayed the greatest formability, while AA5052 exhibited the lowest overall forming ability. The improved formability of the FSW joints suggests the feasibility of solid-state welding for producing dissimilar aluminium sheets that will undergo subsequent forming operations.
- For the 1–5 configuration, the maximum α increased from 0.43 for TIG to 0.94 for FSW, corresponding to an absolute increase of 0.51 and a relative increase of approximately 118.6%. Accordingly, the overall α-range increased from 0.58 to 1.03, representing a 77.6% expansion. For the 3–5 configuration, the maximum α increased from 0.50 to 0.80, corresponding to a 60% increase, while the α-range increased by approximately 28.6%. These results indicate that the influence of the joining process on the accessible strain-path range was more pronounced for the 1–5 configuration.
- The influence of the joining process on the accessible positive strain-path range was more pronounced for the 1–5 configuration than for the 3–5 configuration. The maximum α increased by 125% for FSW 1–5 relative to TIG 1–5, compared with a 60% increase for the 3–5 configuration.
- The results demonstrate that controlling welding-induced microstructural heterogeneity is critical for retaining the forming capability of dissimilar aluminium blanks.

Statements and Declarations

Availability of data and material

The results of this manuscript are a full study, and no data have been fabricated or manipulated to support our conclusions and all of the data are available in the manuscript. Data, text, or theories by others have not been presented unless with references.

Competing interests

The authors have no competing interests to declare that are relevant to the content of this article.

Funding

No funds, grants, or other support was received.

Authors' contributions

Conceptualization: Hamid Reza Rezaei Ashtiani; **Methodology**: Hamid Reza Rezaei Ashtiani and Davood Bagheri; **Formal analysis and investigation**: Hamid Reza Rezaei Ashtiani and Davood Bagheri; **Writing - original draft preparation**: Hamid Reza Rezaei Ashtiani and Davood Bagheri; **Writing - review and editing**: Hamid Reza Rezaei Ashtiani; **Funding acquisition**: Hamid Reza Rezaei Ashtiani and Davood Bagheri; **Resources**: Hamid Reza Rezaei Ashtiani and Davood Bagheri; **Supervision**: Hamid Reza Rezaei Ashtiani

References

1. C. N. Radhika, N. H. Deepak Kumar, and B. Sivasailam, "A review on welding techniques: properties, characterisations and engineering applications," *Advances in Materials and Processing Technologies*, vol. 10, no. 2, pp. 1126-1181, 2023, doi: 10.1080/2374068x.2023.2186638.
2. R. S. Mishra, P. S. De, and N. Kumar, *Friction Stir Welding and Processing: Science and Engineering*. Cham, Switzerland: Springer, 2014.

3. K. Paul, "Controlling factors of forming limit curve: A review," *Advances in Industrial and Manufacturing Engineering*, vol. 2, 2021, doi: 10.1016/j.aime.2021.100033.
4. M. N. S and B. S. Davidson, "Friction stir welding parameters and their influence on mechanical properties of welded AA6061 and AA5052 aluminium plates," *Materials Research Express*, vol. 8, no. 10, 2021, doi: 10.1088/2053-1591/ac2daf.
5. M. Sefat, H. Ghazanfari, and C. Blais, "Friction Stir Welding of 5052-H18 Aluminum Alloy: Modeling and Process Parameter Optimization," *Journal of Materials Engineering and Performance*, vol. 30, no. 3, pp. 1838-1850, 2021, doi: 10.1007/s11665-021-05499-5.
6. P. Reddy and S. Dewangan, " A comparative analysis among the welded Al-6061 plates joined by FSW, MIG and TIG welding methods" *Acta Metallurgica Slovaca*, vol. 29, no. 2, pp. 75-81, 2023, doi: 10.36547/ams.29.2.1778.
7. Khanna, P. Sharma, M. Bharati, and V. J. Badheka, "Friction stir welding of dissimilar aluminium alloys AA 6061-T6 and AA 8011-h14: a novel study," *Journal of the Brazilian Society of Mechanical Sciences and Engineering*, vol. 42, no. 1, 2019, doi: 10.1007/s40430-019-2090-3.
8. Jabraeili et al., "Effect of FSW process parameters on microstructure and mechanical properties of the dissimilar AA2024 Al alloy and 304 stainless steel joints," *Materials Science and Engineering: A*, vol. 814, 2021, doi: 10.1016/j.msea.2021.140981.
9. A. Chularis, R. A. Rzaev, and M. K. Syndetov, "Friction stir welding of aluminium and copper alloys," *Welding International*, vol. 34, no. 4-6, pp. 230-241, 2021, doi: 10.1080/09507116.2021.1906576.
10. Bansal, M. Senthil Kumar, I. Shekhar, S. Chauhan, and S. Bhardwaj, "Effect of welding parameter on mechanical properties of TIG welded AA6061," *Materials Today: Proceedings*, vol. 37, pp. 2126-2131, 2021, doi: 10.1016/j.matpr.2020.07.567.
11. Ahmadi, A. R. Ebrahimi, and A. Hoseinzadeh, "Microstructure Evolution and Mechanical Properties of 2219 Aluminum Alloy A–TIG Welds," *Physics of Metals and Metallography*, vol. 121, no. 5, pp. 483-488, 2020, doi: 10.1134/s0031918x20050026.
12. Samiuddin, J.-l. Li, M. Taimoor, M. N. Siddiqui, S. U. Siddiqui, and J.-t. Xiong, "Investigation on the process parameters of TIG-welded aluminum alloy through mechanical and microstructural characterization," *Defence Technology*, vol. 17, no. 4, pp. 1234-1248, 2021, doi: 10.1016/j.dt.2020.06.012.

13. Vijay, S. Rajanarayanan, and G. N. Ganeshan, "Analysis on mechanical properties of gas tungsten arc welded dissimilar aluminium alloy (Al2024 & Al6063)," *Materials Today: Proceedings*, vol. 21, pp. 384-391, 2020, doi: 10.1016/j.matpr.2019.06.136.
14. Rajendran, K. Srinivasan, V. Balasubramanian, H. Balaji, and P. Selvaraj, "Feasibility study of FSW, LBW and TIG joining process to fabricate light combat aircraft structure," *International Journal of Lightweight Materials and Manufacture*, vol. 4, no. 4, pp. 48